accounts for the near 100% stereochemical bias of the C_5-symmetric corannulene core of **M** in the polymer chain. After observing the notable stereoselectivity of the polymerization in Fig. 3A, we were motivated to investigate whether $\mathbf{M}_{rac}$, a racemic mixture of $\mathbf{M}_R$ and $\mathbf{M}_S$, could be optically resolved by the polymerization using $\mathbf{I}_R$ or $\mathbf{I}_S$ as the initiator (Fig. 3C). Thus, $\mathbf{I}_R$ was added at 25°C to a solution of $\mathbf{M}_{rac}$ (1.0 mM) in MCHex at $[\mathbf{M}_{rac}]_0/[\mathbf{I}_R]_0 = 500$, where in 6 hours the SEC–ultraviolet (UV) profile demonstrated the appearance of a polymeric fraction along with the monomer (Fig. 3D, ii, red). By means of SEC-CD, the polymeric fraction was revealed to possess a positive CD sign at 290 nm, whereas the unassembled monomer fraction possessed a negative CD sign (Fig. 3D, ii, blue). Even upon prolonged reaction for 14 days, the residual monomer observed in 6 hours remained without further consumption (fig. S25A).

For the purpose of quantitatively analyzing the SEC-CD profile in Fig. 3D, we prepared two reference samples, a MCHex solution of nonpolymerized $\mathbf{M}_S$ ($[\mathbf{M}_S]$ = 0.5 mM) and its polymerized version using $\mathbf{I}_R$ as the initiator at $[\mathbf{M}_R]_0/[\mathbf{I}_R]_0 = 250$ ($[\mathbf{M}_S]$ = 0.5 mM). As shown in fig. S25B, the SEC-CD (ii, blue) and SEC-UV (ii, red) traces in Fig. 3D were perfectly reproduced when the corresponding SEC traces of the above reference samples were superimposed. We thus succeeded in optically resolving $\mathbf{M}_S$ and $\mathbf{M}_R$, using initiator $\mathbf{I}_R$ to polymerize only $\mathbf{M}_R$ and vice versa stereoselectively, thus leaving $\mathbf{M}_S$ or $\mathbf{M}_R$ unpolymerized (Fig. 3C). This notable stereochemical selection results from the homochiral nature of the polymer with respect to both the chiral side chains and stacked corannulene units. So far, some chiral monomers are known to self-assemble only homochirally. However, this process yields a racemic mixture of right- and left-hand helical polymers (*26*) because the conventional mechanism does not allow for selection of one enantiomer of the monomer for polymerization. Even for thoroughly studied covalent chain-growth polymerizations, such a high level of optical resolution has been rarely reported (*30*).

In differential scanning calorimetry (DSC), **M** unavoidably polymerizes during the heating process. Upon first heating in DSC (fig. S26, blue), monomeric **M** exhibited an exotherm (20 J g^{-1}) at 82°C and an endotherm at 175°C (27 J g^{-1}). By reference to the DSC profile of polymeric **M** separately prepared (endothermic peak at 177°C, 27 J g^{-1}) (fig. S26, red), the exotherm and endotherm in fig. S26 (blue) are assigned to the thermal polymerization of **M** and dissociation of the resulting polymer, respectively. These DSC profiles corroborate the H-bond stability of **M**, as suggested by comparing its infrared spectrum with that of polymeric **M**. Although the exotherm in the DSC trace indicates that the polymerization is enthalpically driven, the monomer **M** does not spontaneously polymerize without initiator **I** at ambient temperatures because **M** is metastable with a sufficiently large energetic barrier for the self-opening of its intramolecularly H-bonded cage. We presume that the chain growth proceeds through an H-bond–assisted transition state (Fig. 1D), where **M** is preorganized with the growing end of the polymer as well as initiator **I** (both having free amide C=O groups) and transforms its H-bonding mode from intramolecular to intermolecular. This transition state is energetically less demanding than the self-cleavage of the H-bonded amide network in the monomer state. Although the concave structure of the monomer is critical for the present work, further conceptual diversification of metastable monomers for chain-growth supramolecular polymerization may give rise to a paradigm shift in precision macromolecular engineering.

REFERENCES AND NOTES

1. B. Ranby, in *Macromolecular Concept and Strategy for Humanity in Science, Technology and Industry* (Springer, Berlin, 1996), pp. 3–13.
2. H. Staudinger, *Ber. Deut. Chem. Ges.* **53**, 1073–1085 (1920).
3. P. J. Flory, *Principles of Polymer Chemistry* (Cornell Univ. Press, Ithaca, NY, 1969).
4. R. Mülhaupt, *Angew. Chem. Int. Ed.* **43**, 1054–1063 (2004).
5. H. Rehage, H. Hoffmann, *J. Phys. Chem.* **92**, 4712–4719 (1988).
6. N. Zimmerman, J. S. Moore, S. C. Zimmerman, *Chem. Ind.* **1998**, 604–610 (1998).
7. J.-M. Lehn, *Macromol. Chem. Macromol. Symp.* **69**, 1 (1993).
8. J.-M. Lehn, *Supramolecular Chemistry-Concepts and Perspectives* (Wiley-VCH, Weinheim, Germany, ed. 1, 1995).
9. J.-M. Lehn, *Polym. Int.* **51**, 825–839 (2002).
10. R. P. Sijbesma *et al.*, *Science* **278**, 1601–1604 (1997).
11. T. F. A. De Greef *et al.*, *Chem. Rev.* **109**, 5687–5754 (2009).
12. C. Fouquey, J.-M. Lehn, A.-M. Levelut, *Adv. Mater.* **2**, 254–257 (1990).
13. X. Wang *et al.*, *Science* **317**, 644–647 (2007).
14. J. B. Gilroy *et al.*, *Nat. Chem.* **2**, 566–570 (2010).
15. W. Zhang *et al.*, *Science* **334**, 340–343 (2011).
16. S. Ogi, K. Sugiyasu, S. Manna, S. Samitsu, M. Takeuchi, *Nat. Chem.* **6**, 188–195 (2014).
17. G. Odian, *Principles of Polymerization* (Wiley-VCH, New York, ed. 4, 2004).
18. J. Kang *et al.*, *J. Am. Chem. Soc.* **136**, 10640–10644 (2014).
19. Y. T. Wu, J. S. Siegel, *Chem. Rev.* **106**, 4843–4867 (2006).
20. V. M. Tsefrikas, L. T. Scott, *Chem. Rev.* **106**, 4868–4884 (2006).
21. R. Schmidt, M. Stolte, M. Grüne, F. Würthner, *Macromolecules* **44**, 3766–3776 (2011).
22. Y. Ishida, T. Aida, *J. Am. Chem. Soc.* **124**, 14017–14019 (2002).
23. D. Miyajima *et al.*, *J. Am. Chem. Soc.* **131**, 44–45 (2009).
24. P. A. Korevaar *et al.*, *Nature* **481**, 492–496 (2012).
25. M.-I. Childers, J. M. Longo, N. J. Van Zee, A. M. LaPointe, G. W. Coates, *Chem. Rev.* **114**, 8129–8152 (2014).
26. F. Helmich, M. M. J. Smulders, C. C. Lee, A. P. H. J. Schenning, E. W. Meijer, *J. Am. Chem. Soc.* **133**, 12238–12246 (2011).
27. Y. Okamoto, T. Nakano, *Chem. Rev.* **94**, 349–372 (1994).
28. N. Berova, K. Nakanishi, R. W. Woody, *Circular Dichroism: Principles and Applications* (Wiley-VCH, New York, ed. 2, 2000).
29. M. M. J. Smulders *et al.*, *Chirality* **20**, 1016–1022 (2008).
30. W. Hirahata, R. M. Thomas, E. B. Lobkovsky, G. W. Coates, *J. Am. Chem. Soc.* **130**, 17658–17659 (2008).

ACKNOWLEDGMENTS

This work was financially supported by a Grant-in-Aid for Specially Promoted Research (25000005) on "Physically Perturbed Assembly for Tailoring High-Performance Soft Materials with Controlled Macroscopic Structural Anisotropy" for T.A and a Grant-in-Aid for Research Activity Startup (25888024) for D.M.

SUPPLEMENTARY MATERIALS

www.sciencemag.org/content/347/6222/646/suppl/DC1
Materials and Methods
Supplementary Text
Figs. S1 to S27
Tables S1 to S3
References (*31*–*34*)

4 December 2014; accepted 12 January 2015
10.1126/science.aaa4249

ECOLOGICAL FEEDBACKS

Termite mounds can increase the robustness of dryland ecosystems to climatic change

Juan A. Bonachela,[1]* Robert M. Pringle,[1,2] Efrat Sheffer,[1] Tyler C. Coverdale,[1] Jennifer A. Guyton,[1] Kelly K. Caylor,[2,3] Simon A. Levin,[1] Corina E. Tarnita[1,2]†

Self-organized spatial vegetation patterning is widespread and has been described using models of scale-dependent feedback between plants and water on homogeneous substrates. As rainfall decreases, these models yield a characteristic sequence of patterns with increasingly sparse vegetation, followed by sudden collapse to desert. Thus, the final, spot-like pattern may provide early warning for such catastrophic shifts. In many arid ecosystems, however, termite nests impart substrate heterogeneity by altering soil properties, thereby enhancing plant growth. We show that termite-induced heterogeneity interacts with scale-dependent feedbacks to produce vegetation patterns at different spatial grains. Although the coarse-grained patterning resembles that created by scale-dependent feedback alone, it does not indicate imminent desertification. Rather, mound-field landscapes are more robust to aridity, suggesting that termites may help stabilize ecosystems under global change.

Over the past decade, many studies have documented large-scale, spatially periodic clusters of vegetation and other sessile organisms, typically in resource-limited environments (*1*–*4*). Such patterns, found at many levels of biological organization (*5*), can be described by models of scale-dependent feedback (SDF) coupling short-range activation with long-range inhibition (*3*–*9*). For example, in arid and semi-arid savannas and grasslands ("drylands"), plants facilitate neighbors by increasing water infiltration while competing for

water with distant individuals (*10*). In these models, reducing rainfall generates a predictable sequence of patterns with decreasing overall plant biomass: overdispersed gaps, labyrinths, spots, and finally, barren desert. This last transition is known as a "catastrophic shift," or sudden collapse to an unvegetated state (*11*, *12*).

[1]Department of Ecology and Evolutionary Biology, Princeton University, Princeton, NJ 08544, USA. [2]Mpala Research Centre, Post Office Box 555, Nanyuki, Kenya. [3]Department of Civil and Environmental Engineering, Princeton University, Princeton, NJ 08544, USA.
*Present address: Marine Alliance for Science and Technology Scotland (MASTS) Marine Population Modelling Group, Department of Mathematics and Statistics, University of Strathclyde, 26 Richmond Street, Glasgow G1 1XH, Scotland, UK. **†Corresponding author. E-mail: ctarnita@princeton.edu**

The robustness [sensu (*13*), also called resilience (*14*)] of drylands to such catastrophic shifts is an urgent concern given the importance of these systems to human livelihoods [drylands cover >40% of Earth's land surface and are home to >38% of the populace (*15*)] and the increased frequency/intensity of drought expected under climate change (*16*). Scientists have therefore proposed using spotted vegetation patterns, readily identifiable in aerial imagery, as "early-warning signals" of imminent catastrophic shifts (*11*, *12*). However, operationalizing an early-warning system requires mechanistic understanding of both the cause of spotted patterns and the linkage between patterns and robustness; otherwise, "false alarms" could lead to costly resource misallocation (*17*).

Prior SDF models assume soil homogeneity, but most real ecosystems feature heterogeneous substrates. One globally widespread source of heterogeneity is ecosystem engineering by soil-dwelling macrofauna such as termites, ants, and earthworms. Termites are particularly important in savannas of Africa, Australasia, and South America, and their nest structures ("mounds") shape many environmental properties; analogous structures built by ants and burrowing mammals are similarly influential worldwide (*18*). Mound soils differ from surrounding "matrix" soils in physical and chemical composition, which enhances vegetation growth (*19*, *20*), creating "islands of fertility" (Fig. 1) (*20*–*22*). Moreover, mounds are frequently spatially overdispersed

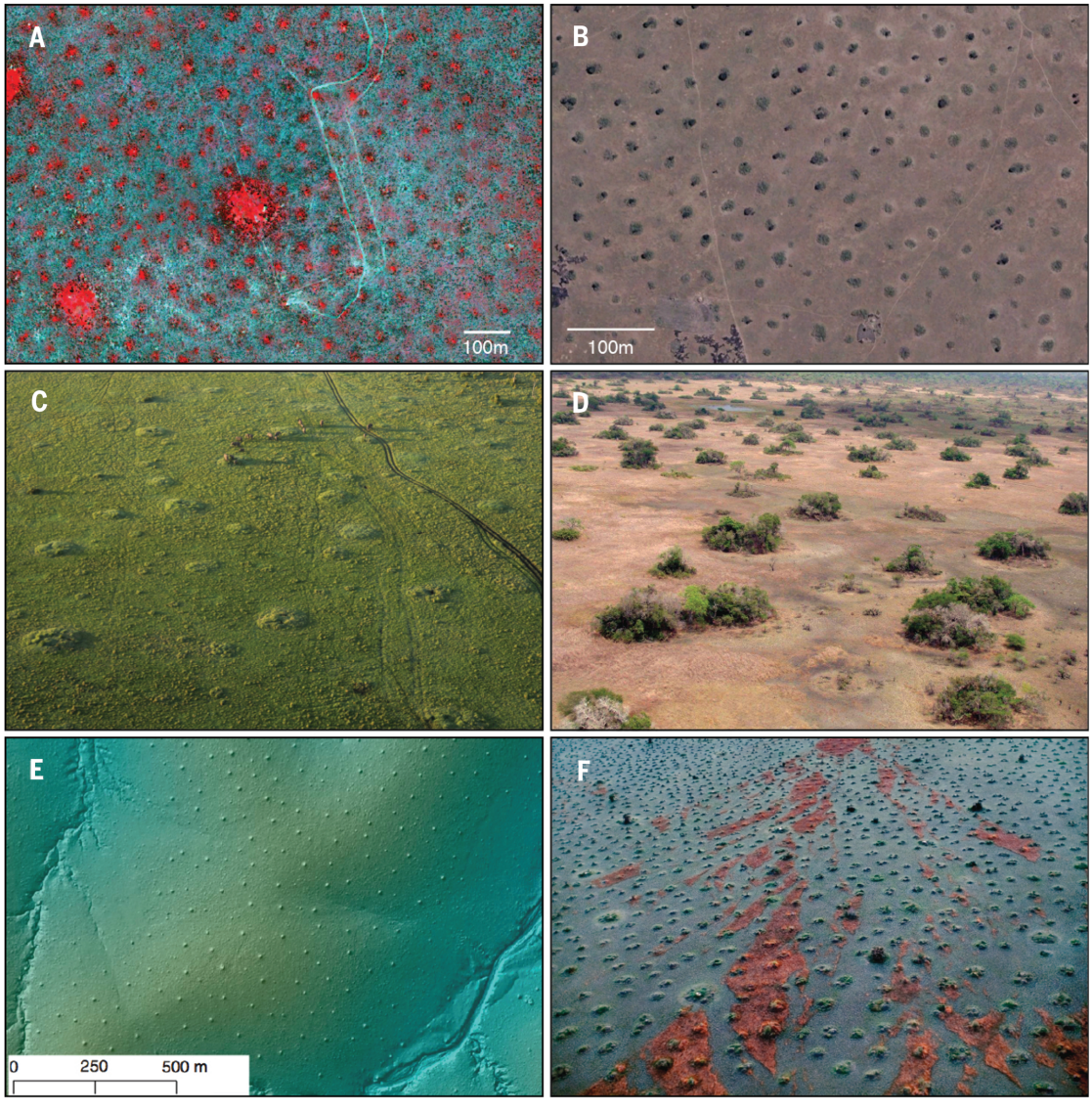

Fig. 1. Patterned termite mounds in real ecosystems. (**A**) False-color infrared Quickbird satellite image (2.4-m resolution) of termite mounds at MRC; mounds appear as small red spots, indicating high primary productivity (larger red patches are abandoned cattle corrals). (**B**) Presumed termite mounds in northwestern Tanzania (–1.29158 latitude, 34.37146 longitude) identified by using Google Earth (2006 image copyright DigitalGlobe). Barren halos are visible around many mounds, as predicted by our model. (**C**) Grass-dominated mounds in Kenya's Masai Mara, taken from hot-air balloon; elephants in the photo provide scale. (**D**) Tree-dominated mounds in Sofala, Mozambique, taken from helicopter (image courtesy of Marc Stalmans). (**E**) Light detection and ranging (LIDAR) hillshade image of termite mounds in South Africa's Kruger National Park, from (*25*). (**F**) Termite mounds on Bangweulu floodplain, Zambia (image courtesy of Frans Lanting).

owing to competition among neighboring colonies (*20*–*25*), which creates spotted vegetation patterns (Fig. 1). The resemblance of these patterns to those predicted by SDF has been noted (*4*, *10*) but not formally analyzed. These two patterning mechanisms are not mutually exclusive and may co-occur.

We modeled SDF on a template of overdispersed termite mounds and tested results against imagery from semi-arid savanna at Kenya's Mpala Research Centre (MRC). Mounds in this system—lenticular humps with belowground chambers and passages (*21*)—are built by fungus-cultivating termites (Macrotermitinae: *Odontotermes*), which are common throughout the Paleotropics. However, our results are applicable to mounds of diverse species and architectures, provided nutrient and/or water availability is elevated either on the mound-proper or in the annular zone around the mound.

We adapt a well-studied three-variable SDF model (*10*) that describes the spatiotemporal dynamics of aboveground vegetation biomass as a function of rainfall (partitioned into runoff and soil water) (*10*, *23*). In traditional two-component SDF models, short-distance enhancement leading to pattern formation usually arises from

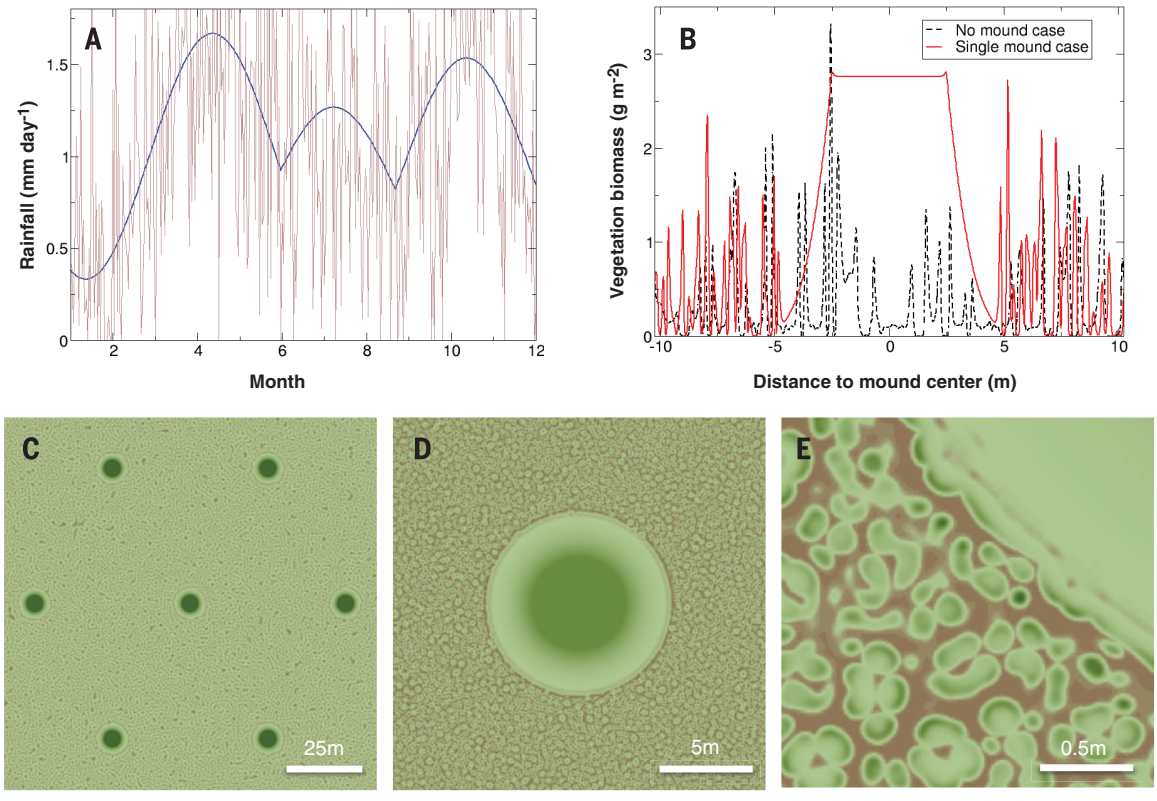

Fig. 2. Vegetation patterns obtained with stochastic rainfall and termite-induced heterogeneity. (**A**) Stochastic rainfall (brown curve) based on observed mean-monthly rainfall (blue curve) at MRC, 1999–2013. (**B**) Transect of predicted vegetation biomass density through a mound (solid curve) and in the absence of mounds (dashed curve). (**C** to **E**) Model outputs showing (C) 123- by 123-m region encompassing seven hexagonally distributed mounds; (D) 20.5- by 20.5-m region with only one mound, showcasing halo effect (for comparison, Fig. 1, B and D); and (E) 2- by 2-m region showing patchy off-mound vegetation and homogeneous on-mound vegetation. Green represents vegetation; brown represents soil. Darker green regions have higher biomass. Parameterization is provided in table S1.

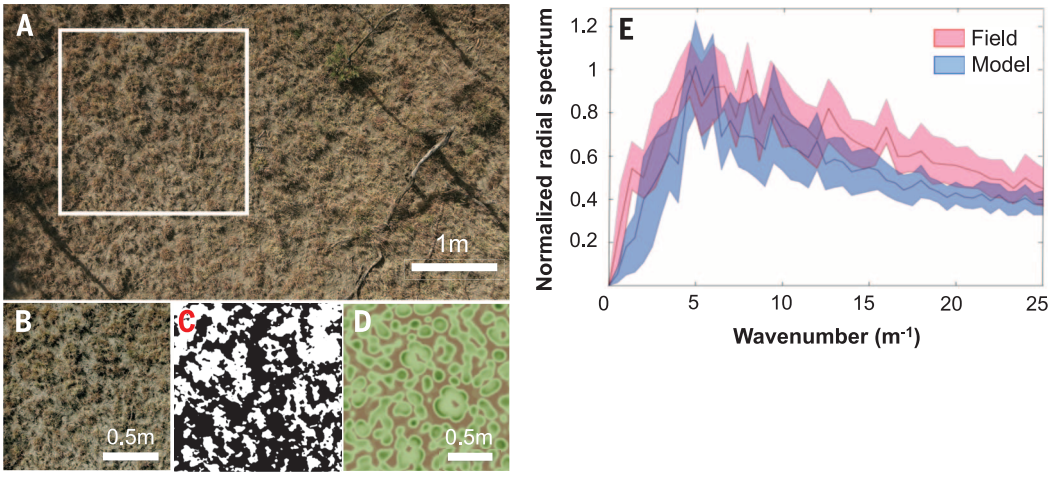

Fig. 3. Correspondence of predicted and observed vegetation patterns. (**A**) Photograph of 3.5- by 6-m region of matrix vegetation taken from 10 m height. (**B**) 1.5- by 1.5-m section used in the analysis, from white square in (A). (**C**) Binary transformation of (B) (white represents vegetation, black represents soil). (**D**) Model output used for comparison, with parameterization as in Fig. 2. (**E**) Normalized radial spectrum of real images (n = 14 samples) and model simulations (n = 192 samples), as a function of wave number.

autocatalysis (positive-feedback) in an "activator" species (*8*, *9*). When more than two components interact, as in the model used here, enhancement can arise indirectly through autocatalytic feedback loops (here, plants–soil water), generating similar pattern morphologies (*26*). We include termite-mound effects in the model by modifying just two parameters. One is the conversion factor c, the efficiency with which plants convert water into biomass ("water-use efficiency"), which we assume is mediated by elevated nutrient availability on mounds (*19*, *27*). The other is the half-saturation constant of water infiltration, k_2, which we modify to account for termites' creation of macropores and alteration of soil texture (*19*, *28*). We leave all other parameters unchanged (table S1) to enable comparison with prior work.

We assume that both nutrient-mediated water-use efficiency and infiltration are elevated on mounds (fig. S1), which is consistent with prior research; specifically, we explore a likely range of on- versus off-mound increases of 0 to 67% for infiltration and 0 to 50% for water-use efficiency (*20*, *23*, *29*). We further assume that termites' effects on water-use efficiency (but not infiltration) are zero-sum: Termites concentrate nutrients on mounds (*27*) but do not increase net nutrient content of the system [this is conservative in terms of finding beneficial effects of termites, and we analyze alternative scenarios in (*23*)]. To assess the effects of rainfall variability, we incorporate seasonality and stochasticity in rainfall based on MRC rainfall records (Fig. 2A).

This modified model yields greater on- than off-mound vegetation biomass (Fig. 2B). Two types of pattern can be identified. One is a coarse-grained lattice of overdispersed vegetation hotspots, reflecting the underlying distribution of termite mounds (*21*), which is exogenous to our model, in conjunction with mounds' positive effects on plant biomass, which is predicted by our model and confirmed with field data from MRC (Fig. 2C) (*23*). The other comprises fine-grained regularity of mound and matrix vegetation resulting from SDF (Fig. 2, D and E). The wavelengths of the fine-grained pattern, both on and off mounds, are determined by local dispersal of plants and diffusion of soil and surface water (*30*) and depend on the values of water-use efficiency and infiltration: Greater values increase vegetation homogeneity; lower values yield regular gaps, labyrinths, and spots, as found in prior SDF models. Thus, the greater the termite-induced improvements in water-use efficiency and infiltration, the more divergent the on- versus off-mound patterning (Fig. 2D and fig. S6). These fine-grained patterns are insensitive to mound distribution (we find equivalent patterns for a single mound and square or hexagonal arrangements), and off-mound patterning is largely insensitive to mound proximity (fig. S3). Our model also produces a "halo" of barren soil at mound edges, resulting from the highly vegetated mound acting as a sink for nearby water, matching observations from various African savannas (Fig. 1, B and D).

To evaluate model predictions of fine-grained patterning, we used Fourier transforms to analyze low-altitude (10 m) aerial photographs of matrix vegetation from MRC (Fig. 3, A to C) (*23*). Off-mound, we find spotted patterns with ~20-cm wavelength, which closely matches the simulated pattern (Fig. 3, D and E). Moreover, as predicted, mound vegetation is both denser (*23*) and more evenly distributed than matrix vegetation (fig. S8). Thus, incorporating termite-induced soil heterogeneity in the SDF framework gives a realistic description of observed patterning. Exact quantitative correspondence is not expected because our analysis uses generic parameter values from prior work (*10*). This model could be further extended to include interactions among plant types (such as trees versus grasses) and/or herbivore impacts, and its predictions could be tested via rain-out/watering experiments.

We next used the modified model to analyze the system's robustness (*13*) to precipitation changes. We consider two components of robustness: "resistance" to perturbation and "recovery" from an undesirable stable state. We find that termite mounds increase ecosystem robustness in three ways (Fig. 4). They enhance resistance, enabling vegetation to persist under substantially reduced rainfall; they reduce the rainfall threshold required for recovery from desert; and they make desertification more gradual (less catastrophic) and thus easier to anticipate and ameliorate. These changes occur because improved infiltration and water-use efficiency on and around mounds enable plants to persist and to repopulate after extirpation, under more arid conditions: Mounds act as refugia for vegetation after the matrix has collapsed to desert.

Sufficient improvement of either water-use efficiency or infiltration can independently increase robustness. As rainfall decreases, two sudden drops in biomass occur (Fig. 4B and figs. S4 and S5). The first (Fig. 4B, i) represents loss of matrix vegetation only and corresponds to total desertification in the system without mounds (Fig. 4A, i). The second (Fig. 4B, ii) represents loss of vegetation from mounds (and hence the entire system) and occurs at lower rainfall, indicating enhanced resistance. As rainfall increases from zero, two sudden jumps in biomass occur (Fig. 4B and figs. S4 and S5): Revegetation of mounds occurs first, at lower rainfall, followed by revegetation of the matrix, indicating enhanced recovery. Insufficient termite-induced improvements yield only one shift, as occurs in the absence of mounds (*10*), and do not enhance ecosystem robustness (fig. S5); in this case, on- and off-mound trajectories are similar. Improving either parameter yields comparable effects, but for our parameter regions, water-use efficiency contributes more to robustness than does infiltration (fig. S5).

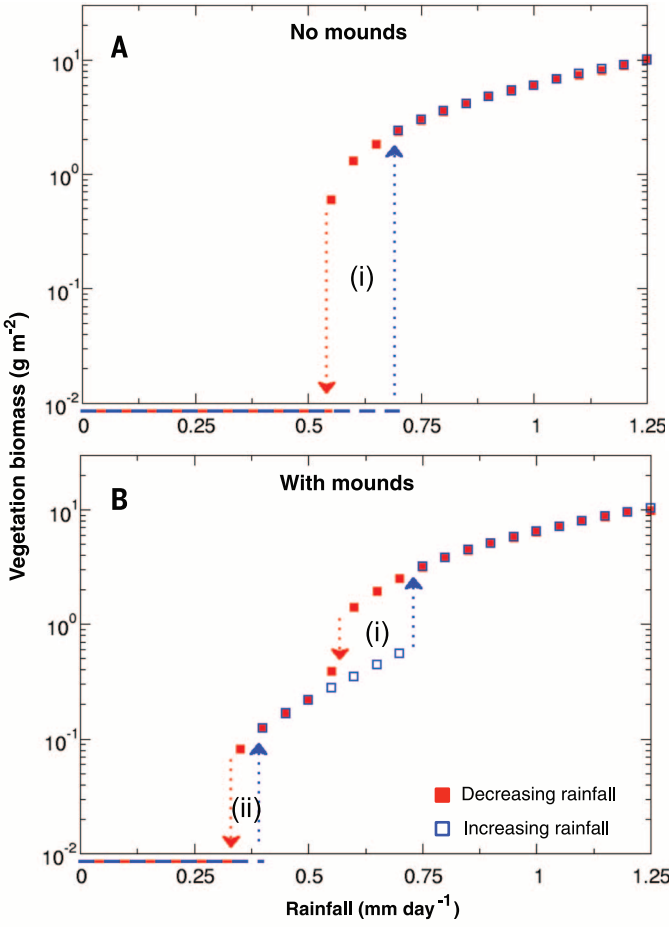

Fig. 4. Termite mounds increase ecosystem robustness. (**A** and **B**) Semilogarithmic phase diagrams under increasing (blue) and decreasing (red) rainfall for (A) model with no termite mounds and (B) the modified model with 50% on- versus off-mound improvement in both growth rate and infiltration efficiency. (A) Without mounds, one hysteresis cycle occurs (i), corresponding to sudden transitions to and from desertification. (B) Adding mounds generates two hysteresis cycles, corresponding to loss/recovery of matrix vegetation (i) and desertification/revegetation (ii). For both (A) and (B), we used fixed rainfall rates and parameters as described in table S1 and fig. S5.

This model describes annual-to-decadal temporal scales, over which precipitation influences the dynamics of vegetation, but not the mounds (*23*). Thus, the model captures pattern evolution and sudden transitions in response to climate-change–induced pulses of drought and rainfall but may not apply if sustained (>50-year) reductions in baseline precipitation cause termite extinction and subsequent homogenization of mound structures. Future theoretical and empirical work is needed to elucidate longer-term dynamic feedbacks between vegetation and mound construction, distribution, and decay.

Our analysis shows that when SDF occurs on a template of overdispersed mounds created by ecosystem engineers, two distinct types of regular patterning coexist at different scales. The fine-grained SDF-generated patterns documented here may be common, but previously unreported because (i) they cannot be observed in available satellite imagery; (ii) even at lower altitudes, grass canopies obscure patterns with centimeter-scale wavelengths; and (iii) stochastic rainfall decreases apparent regularity (compare Fig. 2 and movies S1 and S2 with fig. S3, which assumes constant rainfall). The simplest SDF scenarios typically produce patterns with a single characteristic wavelength (*3*), whereas models combining multiple mechanisms can show complex patterns (*31*, *32*). Thus, co-occurrence of patterns with distinct wavelengths may be a general indicator that multiple mechanisms are operating simultaneously. The mound–SDF interaction is one such route to pattern coexistence and is likely common worldwide because it does not depend on specific mound attributes. Appropriately modified models might therefore inform ongoing debates in which SDF and soil macrofauna are considered alternative hypotheses for particular large-scale patterns, such as Namibian "fairy circles" (*33*, *34*) and various "mima-like mounds" worldwide (*35*).

We further conclude that termites, by creating refugia for plants and nuclei for revegetation, can enhance drylands' resistance to and recovery from drought. These islands of fertility (*20*) appear spot-like in remotely sensed imagery (Fig. 1), but unlike SDF-generated spots, they indicate robustness rather than vulnerability to collapse. These findings confirm the critical links between remotely sensed patterns and ecosystem dynamics but qualify the use of remotely sensed patterning to predict catastrophic shifts. Similar phenomena may occur in other systems in which vegetation patterning is governed by mechanisms that generate apparent SDF dynamics, such as banded vegetation arising from runoff induced by biological crusts on arid hillslopes (*4*, *36*). By such engineering of soil, termites and other ecosystem engineers may buffer the effects of anthropogenic global change in some of the world's most environmentally and socioeconomically sensitive regions.

REFERENCES AND NOTES

1. C. A. Klausmeier, *Science* **284**, 1826–1828 (1999).
2. J. van de Koppel *et al.*, *Science* **322**, 739–742 (2008).
3. M. Rietkerk, J. van de Koppel, *Trends Ecol. Evol.* **23**, 169–175 (2008).
4. V. Deblauwe, P. Couteron, O. Lejeune, J. Bogaert, N. Barbier, *Ecography* **34**, 990–1001 (2011).
5. H. Meinhardt, *Nature* **376**, 722–723 (1995).
6. S. A. Levin, L. A. Segel, *SIAM Rev.* **27**, 45–67 (1985).
7. E. Meron, *Math. Model. Nat. Phenom.* **6**, 163–187 (2011).
8. A. Gierer, H. Meinhardt, *Kybernetik* **12**, 30–39 (1972).
9. P. K. Maini, K. J. Painter, H. Nguyen Phong Chau, *Faraday Trans.* **93**, 3601–3610 (1997).
10. M. Rietkerk *et al.*, *Am. Nat.* **160**, 524–530 (2002).
11. M. Scheffer *et al.*, *Nature* **461**, 53–59 (2009).
12. M. Rietkerk, S. C. Dekker, P. C. de Ruiter, J. van de Koppel, *Science* **305**, 1926–1929 (2004).
13. S. A. Levin, J. Lubchenco, *Bioscience* **58**, 27 (2008).
14. C. S. Holling, *Annu. Rev. Ecol. Evol. Syst.* **4**, 1–23 (1973).
15. J. F. Reynolds *et al.*, *Science* **316**, 847–851 (2007).
16. N. S. Diffenbaugh, C. B. Field, *Science* **341**, 486–492 (2013).
17. V. Dakos, S. Kéfi, M. Rietkerk, E. H. van Nes, M. Scheffer, *Am. Nat.* **177**, E153–E166 (2011).
18. C. Alba-Lynn, J. K. Detling, *Oecologia* **157**, 269–278 (2008).
19. P. Jouquet, S. Traoré, C. Choosai, C. Hartmann, D. Bignell, *Eur. J. Soil Biol.* **47**, 215–222 (2011).
20. G. W. Sileshi, M. A. Arshad, S. Konaté, P. O. Nkunika, *J. Veg. Sci.* **21**, 923–937 (2010).
21. R. M. Pringle, D. F. Doak, A. K. Brody, R. Jocqué, T. M. Palmer, *PLOS Biol.* **8**, e1000377 (2010).
22. A. B. Davies *et al.*, *Ecography* **37**, 852–862 (2014).
23. Materials and methods are available as supplementary materials on *Science* Online.
24. J. Korb, K. E. Linsenmair, *Oecologia* **127**, 324–333 (2001).
25. S. R. Levick *et al.*, *Nat. Commun.* **1**, 1–7 (2010).
26. R. A. Satnoianu, M. Menzinger, P. K. Maini, *J. Math. Biol.* **41**, 493–512 (2000).
27. C. L. Seymour *et al.*, *Soil Biol. Biochem.* **68**, 95–105 (2014).
28. N. Bottinelli *et al.*, *Soil Tillage Res.* **2014**, 1–7 (2014).
29. A. Mando, L. Stroosnijder, L. Brussaar, *Geoderma* **74**, 107–113 (1996).
30. E. Sheffer, J. von Hardenberg, H. Yizhaq, M. Shachak, E. Meron, *Ecol. Lett.* **16**, 127–139 (2013).
31. K. M. Page, P. K. Maini, N. A. Monk, *Physica D* **202**, 95–115 (2005).
32. Q.-X. Liu *et al.*, *Nat. Commun.* **5**, 5234 (2014).
33. N. Juergens, *Science* **339**, 1618–1621 (2013).
34. S. Getzin *et al.*, *Ecography* **37**, 1–11 (2014).
35. M. D. Cramer, N. N. Barger, *Palaeogeogr. Palaeocl.* **409**, 72–83 (2014).
36. O. Malam Issa, J. Trichet, C. Défarge, A. Couté, C. Valentin, *Catena* **37**, 175–196 (1999).

ACKNOWLEDGMENTS

The data are located on the Dryad Digital Repository. This work is a product of U.S. National Science Foundation grant DEB-1355122 to C.E.T., R.M.P., and D. F. Doak. Additional support was provided by the Princeton Environmental Institute (Grand Challenges grant to R.M.P. and C.E.T.), the National Geographic Society (9291 to R.M.P.), the National Science Foundation (EAR-0847368 and DEB-0816453 to K.K.C.), the Andrew W. Mellon Foundation ("Dynamics of South African Vegetation" to S.A.L.), and the John Templeton Foundation (Foundational Questions in Evolutionary Biology RFP-12-14 to C.E.T. and S.A.L.). We thank the Government of Kenya for permission to conduct research; I. Cuesta, D. F. Doak, L. Hedin, R. Martinez-Garcia, J. D. Murray, J. van de Koppel, and T. P. Young for helpful discussions; three anonymous referees for insightful suggestions; K. Grabowski and M. Mohamed for field assistance; and T. P. Young, C. Riginos, and K. Veblen for access to the Kenya Long-term Exclosure Experiment (KLEE), funded by NSF LTREB 12-56034. C.E.T. conceived the study; C.E.T., R.M.P., and J.A.B. developed the theory; J.A.B. analyzed the model; E.S. performed the analysis of pattern in imagery and its comparison with simulation results; R.M.P., T.C.C., and J.A.G. collected field data; S.A.L., K.K.C., and E.S. contributed to discussions of the modeling and analysis; C.E.T., R.M.P., and J.A.B. wrote the first draft of the manuscript; and all authors contributed revisions.

SUPPLEMENTARY MATERIALS

www.sciencemag.org/content/347/6222/651/suppl/DC1
Supplementary Text
Figs. S1 to S8
Table S1
References (*37*–*84*)
Movies S1 and S2

19 September 2014; accepted 16 December 2014
10.1126/science.1261487

PLANT DEVELOPMENT

Genetic control of distal stem cell fate within root and embryonic meristems

Brian C. W. Crawford,[1] Jared Sewell,[2] Greg Golembeski,[1] Carmel Roshan,[1] Jeff A. Long,[2]* Martin F. Yanofsky[1]*

The root meristem consists of populations of distal and proximal stem cells and an organizing center known as the quiescent center. During embryogenesis, initiation of the root meristem occurs when an asymmetric cell division of the hypophysis forms the distal stem cells and quiescent center. We have identified *NO TRANSMITTING TRACT* (*NTT*) and two closely related paralogs as being required for the initiation of the root meristem. All three genes are expressed in the hypophysis, and their expression is dependent on the auxin-signaling pathway. Expression of these genes is necessary for distal stem cell fate within the root meristem, whereas misexpression is sufficient to transform other stem cell populations to a distal stem cell fate in both the embryo and mature roots.

Development of plant roots depends on regulation of stem cell function in the root apical meristem, where the quiescent center separates two populations of stem cells into proximal and distal domains (Fig. 1A) (*1*, *2*). The cells in the quiescent center rarely divide themselves but signal to surrounding stem cells to remain undifferentiated. The quiescent center is formed during embryo development when the uppermost cell of the suspensor, known as the hypophysis, divides asymmetrically to initiate the root meristem. Here we analyze the signals

[1]Division of Biological Sciences, University of California San Diego, La Jolla, CA 92093, USA. [2]Department of Molecular, Cell and Developmental Biology, University of California Los Angeles, Los Angeles, CA 90095, USA.
*Corresponding author. E-mail: marty@ucsd.edu (M.F.Y.); jeffalong@ucla.edu (J.A.L.)